Available online at www.CivileJournal.org

Civil Engineering Journal

(E-ISSN: 2476-3055; ISSN: 2676-6957)

Vol. 12, No. 05, May, 2026

Rockfall Dynamics During Volcanic Eruptive Phases: A Statistical Assessment

Jelena Koritnik [1], Juan C. Santamarta [1], Noelia Cruz-Pérez [1*], Matej Horvat [2], Luis E. Hernández-Gutiérrez [3], Rafael García Martín [4], Sergio Leyva [5]

[1] *Department of Agricultural and Environmental Engineering, Universidad de La Laguna (ULL), San Cristóbal de La Laguna 38200, Spain.*

[2] *Department of Geography, Faculty of Arts, University of Ljubljana, Ljubljana 1000, Slovenia.*

[3] *Instituto Volcanológico de Canarias (INVOLCAN), Puerto de la Cruz 38400, Spain.*

[4] *Department of Security and Emergencies, Cabildo de La Palma, Santa Cruz de la Palma 38700, Spain.*

[5] *College of Forestry and Natural Environment, Universidad Politécnica de Madrid (UPM), Madrid 28031, Spain.*

Received 19 November 2025; Revised 19 April 2026; Accepted 23 April 2026; Published 01 May 2026

Abstract

The Canary Islands, a volcanic archipelago off the northwest coast of Africa, are frequently exposed to geohazards. The 2021 Tajogaite eruption on La Palma provided an opportunity to assess how volcanic activity and related seismicity influence rockfall dynamics. This study statistically analyzed a dataset of 1,111 road-related rockfall incidents recorded between 2019 and 2024, comparing event occurrence, severity, and lithological distribution across pre-, syn-, and post-eruption periods. Events were classified based on operational descriptors, and linked to geological units to evaluate lithological controls. While the total number of events remained nearly identical before (519) and after (517) the eruption, the normalized rate of rockfall occurrence increased during the eruptive phase. Lithological distributions also differed across periods: altered basalts consistently recorded the highest number of incidents; pyroclasts and colluvium increased syn-eruption likely due to seismic shaking; and fresh basalts declined post-eruption, suggesting prior mobilization of unstable material. This study provides empirical insight into how eruptive processes influence infrastructure-related rockfall hazards on volcanic islands characterized by steep topography and narrow, low-redundancy mountain road networks. Nevertheless, rockfalls also occurred consistently during non-eruptive periods, highlighting the need for continuous slope hazard monitoring in environments such as La Palma where both eruptive and non-eruptive processes threaten exposed infrastructure, population, and high tourist activity.

Keywords: Volcanic Archipelago; Seismic Activity; Geohazards; Spatial Analysis; Lithology; Severity.

1. Introduction

Rockfalls are rapid gravitational movements of detached rock blocks and fragments from steep slopes, constituting a widespread form of slope instability [1]. Due to their rapid onset and high kinetic energy, such events can threaten human life and damage infrastructure [2, 3]. Transport corridors are particularly exposed, as roads frequently traverse unstable terrain or are excavated directly into rock masses [4, 5]. In this context, we adopt the definition of a hazard as a natural process or phenomenon that may cause loss of life, property damage, or social and economic disruption [6]. Accordingly, geological processes such as rockfalls are considered hazards only when they pose a threat to human systems.

* Corresponding author: ncruzper@ull.edu.es

https://doi.org/10.28991/CEJ-2026-012-05-014

Substantial infrastructure damage, economic losses, and disruption of transportation networks associated with rockfall occurrences have been documented worldwide [7–11], particularly in mountainous regions such as the Alps [12–14], the Himalayas [15–17], and the Andes [18, 19]. Comparable impacts are observed in volcanic island environments such as the Canary Islands [20], where steep volcanic terrain, constrained road networks, and intense tourism-related traffic increase exposure to rockfall hazards.

Rockfall occurrence is controlled by internal factors related to rock mass and slope properties and external factors capable of triggering detachment [8, 21]. Internal factors include lithology, rock strength, joints and fractures, fault density, weathering properties, block size and geometry, and slope inclination, which together influence rockfall susceptibility [9]. External factors may trigger rockfall detachment, including intense rainfall [22], freeze–thaw cycles [23, 24], earthquakes and seismic shaking [25], erosion [8], and anthropogenic disturbances [26]. Seismic shaking is widely recognized as a trigger of rockfalls and other slope failures [27–30]. Earthquake-induced rockfalls represent an important secondary hazard within multi-hazard scenarios, as ground shaking associated with the propagation of seismic waves can destabilize fractured rock masses and initiate both co-seismic and post-seismic rockfall activity [31]. In some earthquakes, losses associated with these secondary hazards exceed those caused directly by the seismic event [32]. Low-magnitude earthquakes, when combined with rainfall or occurring as seismic swarms that produce repetitive shaking, can trigger slope instabilities through progressive damage of fractured slopes [33, 34].

Volcanic regions commonly experience seismic swarms and repeated low-magnitude earthquakes associated with magma migration and volcanic unrest, which can increase slope instability and promote rockfalls before, during, and after eruptions [25, 35, 36]. Volcanic slopes are also characterized by steep relief and heterogeneous volcanic lithologies, where volcanic rocks exhibit strong geomechanical heterogeneity and anisotropy, including voids, cavities, alternating strata of different competences, and discontinuities of varied thermal, mechanical, and erosional origin [37]. These characteristics favor rockfalls and other mass-wasting processes affecting volcanic terrains [38]. Slope instability in volcanic environments often results from the combined action of several conditioning and triggering processes, including magma emplacement, stress changes, pore-pressure variations, seismic activity, and hydrothermal alteration [38, 39].

Previous studies have examined rockfalls associated with volcanic unrest and eruptive activity both as precursory signals and as outcomes, including dome growth, pyroclastic activity, lava emplacement, and volcanic seismicity [35, 36, 40]. In volcanic environments like the Canary Islands, rockfalls and landslides are frequently associated with intense precipitation, strong winds, thermal dilation associated with solar radiation, and seismicity linked to volcanic eruptions [41]. Rockfalls occur frequently in the archipelago and cause significant economic losses along the road network and in urban areas [42]. Exposure to rockfall hazards is further amplified by steep volcanic cliffs, constrained infrastructure networks, and continued urban expansion into areas prone to mass movements.

Related regional studies include citizen science monitoring initiatives [43, 44]; rainfall-induced rockfalls in Tenerife using operational road maintenance records [22]; geomechanical assessment of volcanic slopes and the development of volcano-specific slope assessment indices [37]; geotechnical simplification and road-focused hazard assessment in Gran Canaria [45]; and susceptibility and source-area modeling in El Hierro, where the 2011–2012 submarine volcanic eruption triggered numerous rockfalls near the Los Roquillos tunnel, a critical transport infrastructure [46, 47]. Beyond slope instability studies, infrastructure-focused analyses have shown that volcanic eruptions generate multiple hazards, including lava, tephra, and gas, whose interaction with low-redundancy insular infrastructure can produce cascading impacts across transport networks and other critical systems [48].

Taken together, previous research has primarily examined rockfall triggers, slope susceptibility and source-area identification, and geomechanical behavior of volcanic slopes. However, the temporal evolution of rockfall hazards during volcanic unrest and eruption sequences remains poorly quantified, particularly whether rockfall occurrence changes before, during, and after eruptions when assessed using multi-year operational incident datasets, and whether these patterns vary with lithological context. On active volcanic islands, where transport networks have limited redundancy and rockfall activity directly affects accessibility, emergency operations, and continuity of essential services, understanding the temporal dynamics of rockfall hazards is essential for both monitoring and risk management [49].

La Palma provides a particularly suitable setting to investigate these dynamics, as the island is characterized by steep volcanic relief, intense erosional incision, and a road network strongly constrained by topography. Its most recent eruption, the 2021 Tajogaite eruption of Cumbre Vieja, lasted 85 days and was preceded and accompanied by seismic activity [50, 51]. Previous studies of the Tajogaite eruption have documented volcanic hazards, including lava flows, tephra fall, and volcanic gas emissions, and their impacts on groundwater, infrastructure, land cover, and socio-environmental systems through cascading disruptions across the island [52–59].

The eruption was preceded by a seismic swarm and followed by a prolonged post-eruptive adjustment period, providing a unique temporal framework to examine rockfall hazards across successive pre-, syn-, and post-eruptive

stages. In addition, the lithological heterogeneity of La Palma, including fresh basalts, altered basalts, pyroclastic deposits, and volcanic or volcano-sedimentary units, provides a strong basis for assessing lithological controls on rockfall dynamics.

This study is based on incident reports compiled by the Centro de Coordinación Operativa Insular (CECOPIN) of La Palma. From this operational database, rockfall incidents recorded between 2019 and 2024 were identified and compiled into a structured dataset of 1,111 events affecting roads and accessible paths. Because the database primarily records incidents requiring operational response, it captures rockfalls affecting infrastructure and mobility rather than the full range of slope failures occurring in remote or inaccessible areas of the island that may not pose a direct hazard. The statistical analysis examines how recorded rockfall occurrence and incident characteristics evolved across the pre-, syn-, and post-eruptive phases of the 2021 Tajogaite eruption, evaluates whether these temporal patterns vary according to lithological context, and assesses changes in descriptor-derived severity and associated impacts on infrastructure and exposed populations.

The study brings together three dimensions that are rarely analyzed jointly: volcanic eruption processes, lithological controls on rockfall occurrence, and road rockfall inventories. It aims to quantify changes in rockfall occurrence associated with eruptive activity, relate recorded events to geological units, and evaluate their implications for road infrastructure and public safety, providing a quantitative basis for hazard assessment and infrastructure planning on La Palma and comparable volcanic islands.

2. Methodology

2.1. Study Area

The Canary Islands archipelago lies in the Atlantic Ocean, about 100 km off the northwestern coast of Africa. La Palma, one of the seven volcanic islands, is the fifth largest and the second highest in the archipelago. The island covers 708 km² and reaches a maximum elevation of 2,430 m a.s.l. La Palma has a pronounced north-south orientation and is comprised of two main volcanic units: the northern shield volcano and the southern volcanic ridge of Cumbre Vieja, which is currently considered the most volcanically active sector of the archipelago. The island has an average slope of 24.03º, and its steep relief promotes intense erosion and slope processes. The most recent volcanic eruption on La Palma began on September 19, 2021 and lasted 85 days, ending on December 13, 2021 [51] (Figure 1).

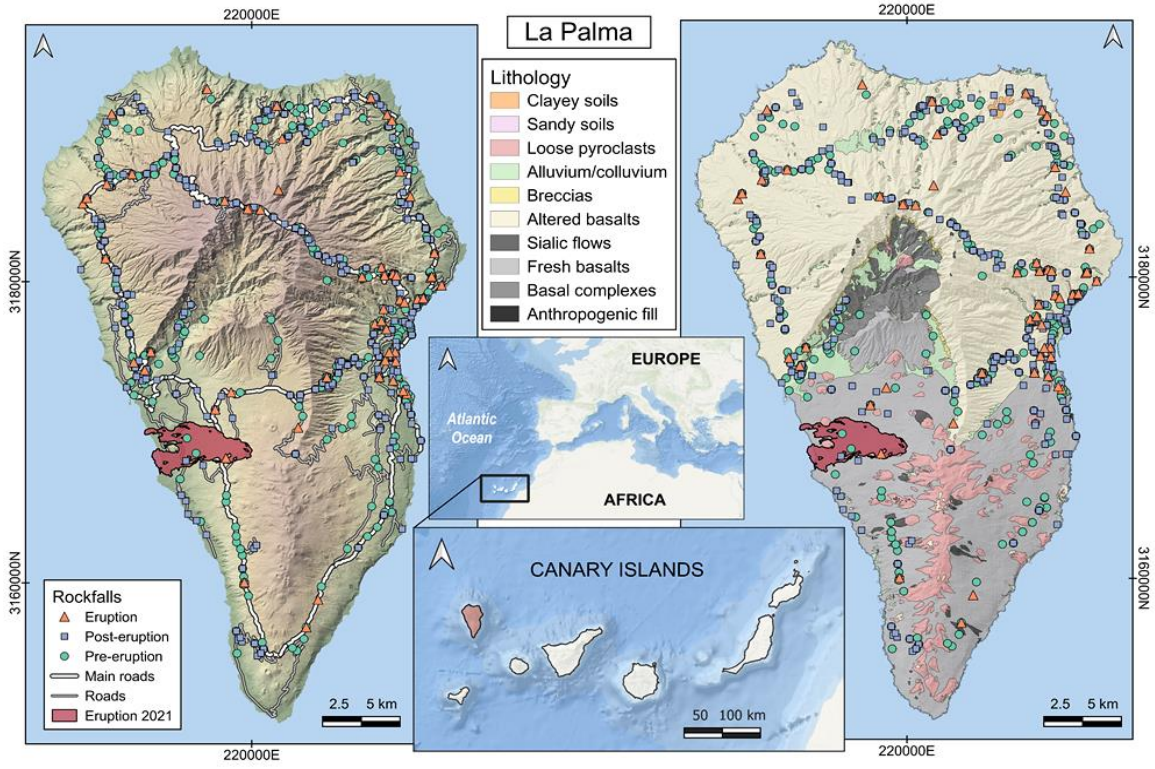

Figure 1. Spatial distribution of rockfall events on La Palma (Canary Islands) before, during, and after the 2021 volcanic eruption, overlaid on topographic and lithological basemaps (IDECanarias). The 2021 eruption layer represents lava flows produced (CRS: WGS 84/UTM 28N).

2.2. Dataset Description and Processing

Rockfall events were compiled from operational reports provided by the Centro de Coordinación Operativa Insular (CECOPIN) of La Palma, which systematically documents incidents reported by emergency services and municipal authorities. These records include all incidents requiring operational response or removal of rock material from roads and accessible paths, whether performed directly by emergency services or coordinated through municipal authorities, resulting in a consistent operational record of road-affecting rockfall events. From this database, covering the period from 1 January 2019 to 7 May 2024, all entries referring to rockfall-related events were identified and extracted (e.g., *desprendimiento* (D), *derrumbe* (DR), *piedras* (P)), while non-geological incidents (e.g., dead animals, oil spills, traffic accidents, and other non-geological events) were excluded (Figure 2).

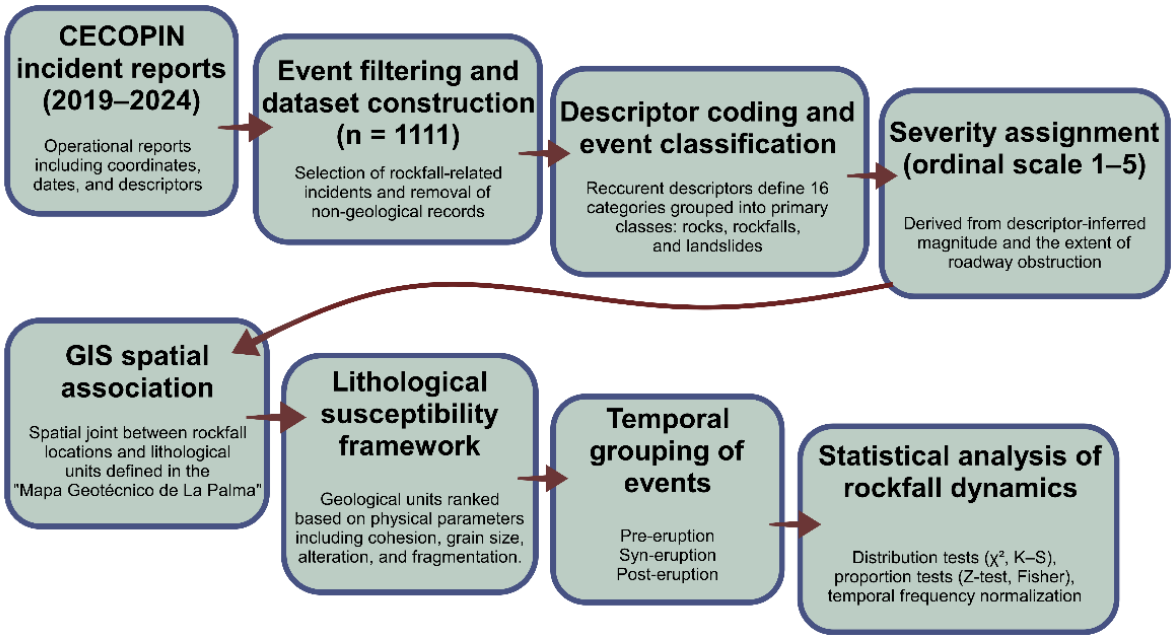

Figure 2. Workflow of the methodological framework used to process the CECOPIN incident reports

Following this filtering procedure, the resulting dataset comprised 1,111 operational records corresponding to rockfall-related incidents. Of these, eight records (all from the pre-eruption period) lacked geographic coordinates. During dataset preparation, records were identified, filtered, georeferenced, and transformed into a structured analytical dataset. All subsequent data processing, descriptor coding, categorization, and spatial analysis were conducted using Python 3 (including the libraries Pandas, NumPy, SciPy, Statsmodels, and Matplotlib) and QGIS 3.40.

Each CECOPIN record includes incident location, date and time, and a brief description provided by operational technicians at the time of reporting. Descriptors ranged from single terms such as "*desprendimiento*" (rockfall) to more detailed accounts including block size, detached rock mass volume, roadway obstruction, and whether machinery was required for clearance. Because these records were consistently formatted in Spanish, recurrent descriptors were extracted to develop a coding system. For example, P (*piedras*) referred to individual rocks, PO (*piedras ocupan carril*) to rocks obstructing a lane, and DPGO (*desprendimiento con piedras grandes ocupando carril*) to a rockfall with large boulders blocking the roadway. This procedure transformed the 1,111 rockfall records into a set of distinct incident categories, which were then translated into English event types.

In total, sixteen geologically relevant categories were defined (Table 1), based on the type of mass movement and the characteristics of the detached material described in the CECOPIN reports. The categorization considered the material's composition and block size, and, when relevant, whether the incident caused significant road obstruction. The resulting categories span from isolated rock detachment and minor rockfalls, through mass movements of varying magnitude, to large-scale landslides involving large boulders. Table 1 lists these categories together with their associated codes derived from Spanish descriptors (event code), and presents them in ranked order, from the lowest-impact category (rocks) at the bottom to the highest-impact category (landslide with large boulders affecting roadway) at the top, reflecting the hazard-oriented logic of the scheme.

Table 1. Rockfall events categorization and severity assessment

Category	Severity	Severity code	Class	Event code
Landslide with large boulders affecting roadway	Very high	5	Landslide	DROPG
Large landslide	Very high	5	Landslide	DRG
Large rockfall affecting roadway	Very high	5	Rockfall	DGO
Rockfall with large boulders affecting roadway	Very high	5	Rockfall	DPGO
Landslide with large boulders	High	4	Landslide	DRPG
Large rockfall	High	4	Rockfall	DG
Rockfall with large boulders	High	4	Rockfall	DPG
Landslide affecting roadway	Moderate	3	Landslide	DRO
Landslide	Moderate	3	Landslide	DR
Rockfall affecting roadway	Moderate	3	Rockfall	DO
Rockfall	Moderate	3	Rockfall	D
Very large rock	Low	2	Rocks	PGG
Large rock(s) affecting roadway	Low	2	Rocks	PGO
Large rock(s)	Low	2	Rocks	PG
Rock(s) affecting roadway	Very low	1	Rocks	PO
Rock(s)	Very low	1	Rocks	P

Following the event categorization, each record was assigned a severity code derived from the operational descriptors contained in the CECOPIN reports. Because the original records consist of qualitative field descriptions rather than quantitative measurements, severity was defined using an ordinal, descriptor-based scale intended to approximate the relative magnitude of the event. Higher codes indicate greater overall hazard severity, but gaps between ranks are not assumed equal. The classification primarily reflects the inferred physical scale of the slope process, based on descriptors indicating block size, estimated volume, and the extent of material mobilization. Consequences were generally not used to determine severity, as impacts on vehicles or infrastructure may depend on chance exposure rather than process magnitude. However, roadway obstruction was used to distinguish the highest severity level when descriptors indicated failures producing significant blockage. The resulting severity variable should therefore be interpreted as an indicative proxy of event magnitude rather than a direct quantitative measure. In this context, the severity scale is used as a supporting indicator to explore potential variations in event magnitude across the study period rather than as a primary metric of analysis.

Based on this rationale, we established a five-level rockfall severity scale (Table 2). The scale is ordinal and primarily reflects the inferred magnitude of the slope process from CECOPIN descriptors, which are treated as indicative rather than quantitative. It ranges from very low (code 1) for isolated small rocks consistent with minimal slope instability to very high (code 5). Events at the highest level are those whose descriptors indicate the greatest slope instability; where instability was comparable, levels 4 and 5 were separated by reported roadway obstruction. Because the descriptors are operational notes rather than measurements, obstruction alone did not determine severity and occurs at lower levels as well. Intermediate levels capture gradations between these end members, including clustered rockfalls, very large blocks (car-sized), and accumulations of detached rock fragments indicative of localized slope failure. This procedure produced a consistent severity classification that was applied to all geologically induced road incidents in the dataset.

Table 2. Severity classification and descriptions of categories

Severity	Description
Very high (5)	Descriptors indicate the greatest slope instability and largest mobilized volumes: either a large landslide, or a rockfall/landslide involving large or very large boulders with reported roadway obstruction
High (4)	Rockfall or landslide described as large or involving large boulders, without reported roadway obstruction
Moderate (3)	Rockfall or landslide without size qualifiers, with or without roadway obstruction
Low (2)	Large rocks present but no rockfall or landslide process indicated
Very low (1)	Isolated small rocks with minimal evidence of slope instability

2.3. Geological Unit Association

In this study, geological units were assigned by performing a spatial join in QGIS between the shapefile of rockfall-related events, and the official geological map of La Palma (Mapa Geotécnico de La Palma; Open Data La Palma). This operation produced a single attribute table in which each event was associated with its corresponding lithological unit. The geological units are identified by a unit code, terrain group, full description, and short name. A complete listing of these units is provided in Table 3.

Table 3. Geological units present in the study area, with identifiers and descriptions

Unit	Group	Description	Lithology
I	T3	Cretaceous sediments, submarine lavas, plutonic rocks (gabbros, syenites), high dike density	Basal complexes
II	T1	Sialic lava flows and massifs	Sialic flows
III	T3	Altered basaltic massifs; alternating compact basalt layers	Altered basalts
IV	T1-T3	Fresh basaltic flows; aa or pahoehoe types, scoriaceous or with cavities	Fresh basalts
V	T3	Loose or weakly cemented pyroclastic materials	Loose pyroclasts
VI	T2	Breccia formations; chaotic compact breccias of mono/polymictic nature	Breccias
VII	T3	Alluvial and colluvial deposits along ravines	Alluvium/colluvium
VIII	T3	Sandy soils; marine or aeolian sand deposits	Sandy soils
IX	T3	Clayey and/or silty soils; residual or lacustrine fine detrital material	Clayey soils

To evaluate the relative susceptibility of geological units to slope failures, an ordinal ranking system was developed based on four key geological attributes: (1) material cohesion and degree of lithification; (2) grain-size characteristics and permeability; (3) intensity of chemical or hydrothermal alteration; and (4) structural fragmentation or brecciation. Unconsolidated pyroclastic deposits and alluvial-colluvial materials received the highest susceptibility scores, whereas fresh basaltic lava flows and crystalline basement complexes were assigned the lowest (Table 4). This classification represents a qualitative susceptibility ranking based on the geological attributes described above and is used here as a conceptual framework for interpreting the lithological context of recorded events. In this context, susceptibility refers to the likelihood that a given area may experience a particular hazard based solely on conditioning factors, without considering event frequency or consequences [60].

Table 4. Lithological susceptibility ranking framework

Susceptibility	Lithology	Description
very high (4)	Loose pyroclasts	Unconsolidated or weakly cemented deposits with low cohesion, highly prone to rapid slope failure
	Alluvium/colluvium	
high (3)	Clayey soils	Fine-grained soils that lose shear strength when saturated or under changing pore-pressure conditions
	Sandy soils	
moderate (2)	Altered basalts	Cohesive rock masses weakened by alteration or fragmentation; moderate shear strength but localized failure risk
	Breccias	
low (1)	Sialic flows	Well-lithified, competent volcanic and plutonic rocks with high strength and minimal inherent instability
	Fresh basalts	
	Basal complexes	

3. Results and Discussion

3.1. Statistical Analysis, Severity and Rockfall Event Class Assessment

A temporal comparison of rockfall event counts was conducted across three periods: pre-eruption, during the eruption, and post-eruption. The eruption period was defined using the official start and end dates of the 2021 Tajogaite eruption (19 September–13 December 2021). The dataset includes 519 rockfall events recorded during the 982-day pre-eruption period (~32.3 months), 75 events during the 85-day syn-eruption period (~2.8 months), and 517 events during the 876-day post-eruption period (~28.8 months).

To examine severity distribution, rockfall events assigned a severity level 4 or 5 were analyzed separately. These represent the highest categories within the operational descriptor-based severity scale. Such events accounted for 4% of all records in the pre-eruption period (21 out of 519), 13% syn-eruption (10 out of 75), and 8% in the post-eruption period (39 out of 517). Summary statistics for severity in each period are presented in Table 5. Mean severity values were 2.31, 2.79, and 2.43 for the pre-, syn-, and post-eruption phases, respectively, while the median severity remained constant at 3 across all periods.

Table 5. Summary statistics of rockfall event severity across pre-eruption, syn-eruption, and post-eruption periods

Period	Count	Mean severity	Median
Pre-eruption	519	2.31	3
Eruption	75	2.79	3
Post-eruption	517	2.43	3

The frequency distribution of rockfall event severities was analyzed for the pre-, syn-, and post-eruption periods. Severity levels (1–5) were compared using a grouped bar chart in which the distribution for each period was normalized to 100% (Figure 3). During the eruption period, the relative proportion of mid- to high-severity categories (levels 3–5) increases, while lower-severity events (levels 1–2) decrease. In the post-eruption period, the distribution shifts toward the pre-eruption pattern but retains a higher relative frequency of higher-severity categories compared to the baseline. Because severity is inferred from qualitative operational descriptors rather than direct measurements, some uncertainty in the assignment of severity levels cannot be excluded. The statistical comparisons presented should therefore be interpreted as indicative patterns in rockfall event magnitude rather than precise quantitative differences.

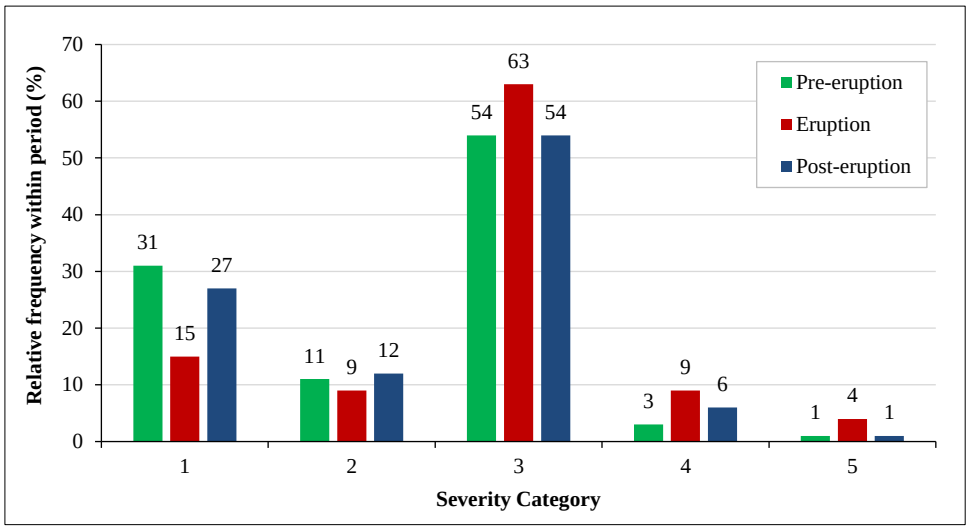

Figure 3. Proportional severity distribution of rockfall events during pre-eruption, eruption, and post-eruption periods

To assess whether rockfall severity differed among pre-, syn-, and post-eruption periods, several statistical analyses were performed. A Chi-square test of independence was conducted on a 3×5 contingency table of event counts across five severity categories (1–5) within each period to evaluate whether severity distribution differed among the three periods. Pairwise Kolmogorov–Smirnov (K–S) tests were then used to compare the distributions of severity scores between periods. To examine whether the proportion of high-severity rockfall events (severity levels 4 and 5) differed among periods, a 3×2 contingency table was analyzed using a Chi-square test of independence. Pairwise differences between periods were evaluated using two-proportion Z-tests. Fisher's exact tests were additionally performed to verify results in comparisons involving small sample sizes.

The Chi-square test on Period × Severity contingency table (3×5) yielded a Chi-square statistic of $\chi^2 = 21.99$ (df = 8, where df denotes degrees of freedom) with a p-value of 0.005, indicating that the overall distributions of severity levels differ significantly across the pre-, syn-, and post-eruption periods.

Pairwise Kolmogorov–Smirnov tests were then applied to compare severity distributions between periods. The Kolmogorov–Smirnov statistic (D) and corresponding p-values were:

(i) Pre-eruption vs. syn-eruption: D = 0.18, p = 0.02

(ii) Pre-eruption vs. post-eruption: D = 0.045, p = 0.64

(iii) Syn-eruption vs. post-eruption: D = 0.15, p = 0.11

These results indicate a statistically significant difference only between the pre- and syn-eruption severity distributions, whereas differences between pre- and post-eruption, and between syn- and post-eruption, were not statistically significant.

The Chi-square test on the Period × High-severity contingency table (severity levels 4 –5) yielded $\chi^2 = 12.1$ (df = 2, p = 0.002), indicating a statistically significant difference in the proportion of high-severity events across the pre-, syn-, and post-eruption periods.

(i) Pairwise comparisons of high-severity event proportions were conducted using two-proportion Z-tests (Z denotes the test statistic). Fisher's exact tests were also calculated, and the corresponding odds ratios (OR) are reported below: Pre-eruption vs. syn-eruption: Z = -3.4, p = 0.001; Fisher's exact OR = 3.7, p = 0.003

(ii) Pre-eruption vs. post-eruption: Z = -2.4, p = 0.02; OR = 1.9, p = 0.02

(iii) Syn-eruption vs. post-eruption: Z = 1.7, p = 0.09; OR = 0.5, p = 0.11

These results indicate that the proportion of high-severity events was significantly higher during the eruption compared with the pre-eruption baseline, and also higher in the post-eruption period relative to the pre-eruption period. In contrast, the difference between the syn- and post-eruption periods was not statistically significant, suggesting that the higher proportion of high-severity categories may have continued beyond the eruption but was not statistically different between those two periods.

Because rockfall incidents may occur in short-term clusters related to common triggering conditions, strict independence of observations cannot be fully guaranteed; therefore, the statistical comparisons presented here should be interpreted as indicative patterns rather than strictly independent realizations.

Together, these statistical analyses indicate that the distribution and proportion of high-severity categories of rockfall incidents differed significantly across the three study periods. This suggests that the eruption was associated with a shift toward potentially more severe rockfall incidents, and that this pattern may have partly continued into the post-eruption period.

A proportional frequency analysis of rockfall event classes was conducted across the pre-eruption, syn-, and post-eruption periods to identify temporal changes in the distribution of event classes. Event counts per class were normalized by the total number of events in each period to obtain class-wise percentages, allowing comparison across periods despite differences in sample size. The analysis revealed the following trends (Figure 4):

(i) Landslide events increased from 7% of total events in the pre-eruption period to 10% in the post-eruption period, representing a +3 percentage point change (relative increase of 43%). A pronounced peak occurred during the eruption period, reaching 15% (+8 percentage points relative to pre-eruption).

(ii) Rockfall events remained relatively stable overall, accounting for 51% of events in both the pre- and post-eruption periods. However, a temporary increase of +10 percentage points occurred during the eruption before returning to pre-eruption levels.

(iii) Rocks (isolated blocks or fragments) decreased from 42% in the pre-eruption period to 39% post-eruption, representing a -3 percentage point change (relative decrease of 7%). The eruption period showed a marked reduction in this class.

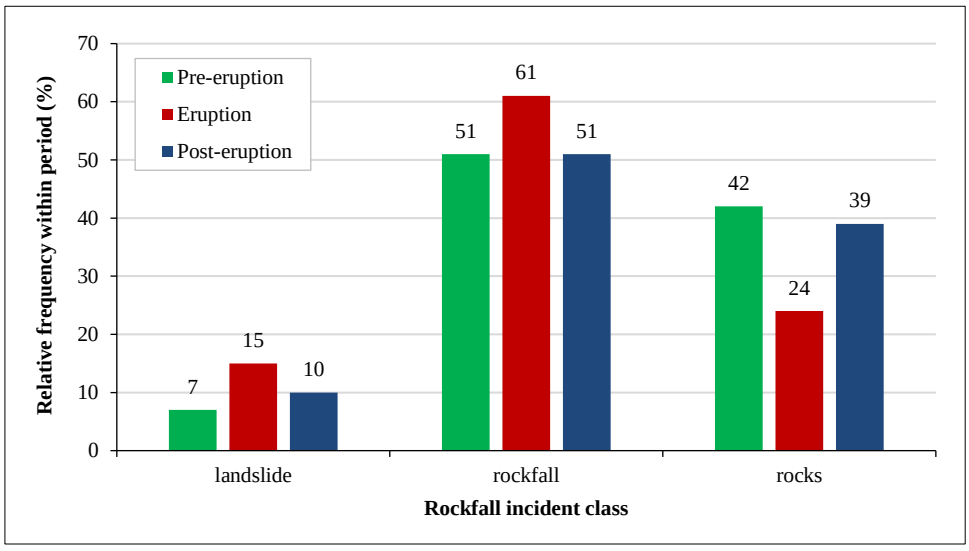

Figure 4. Percentage of rockfall events by event class during pre-eruption, syn-eruption, and post-eruption periods

In this study, rockfall hazard is considered in relation to its potential impact on infrastructure and population. The analyzed inventory consists of operational incident reports, which primarily document events affecting roads and accessible paths rather than slope failures occurring in remote areas. This infrastructure-oriented perspective is consistent with the objective of the study, which focuses on rockfalls that disrupt transport corridors and require operational response.

Within this context, roadway obstruction was considered when distinguishing the severity classification, as it reflects the scale of disruption to infrastructure and mobility. Obstruction typically implies traffic interruption, detours, clearance operations, or the use of heavy machinery, all of which increase the operational impact of the event. This consideration is particularly relevant for La Palma, where the road network is strongly constrained by steep volcanic topography. Roads are commonly excavated directly into rock slopes and are typically narrow two-direction corridors with limited redundancy. Consequently, rockfalls frequently occur directly onto roadways and can rapidly disrupt mobility.

These impacts are amplified by the high importance of road accessibility for both residents and visitors. The Canary Islands constitute one of the most visited tourist regions in Europe, and La Palma receives substantial visitor traffic relative to its road capacity. Temporary road closures or lane blockages can therefore propagate operational disruptions across the transport network [48], increasing the societal relevance of rockfalls affecting road corridors [61–63].

3.2. Temporal Analysis

To examine seasonal patterns in rockfall activity, monthly frequencies were compared across the pre-, syn-, and post-eruption periods (Figure 5). Because the dataset is based on operational incident reports, the recorded frequencies may partly reflect reporting practices rather than true event occurrence; however, as rockfalls on La Palma commonly affect narrow and low-redundancy roads, and disrupt traffic, they are generally reported, although during the eruption reporting may have been influenced either by heightened alertness or by habituation to emergency conditions, so the observed temporal patterns should be interpreted with this limitation in mind.

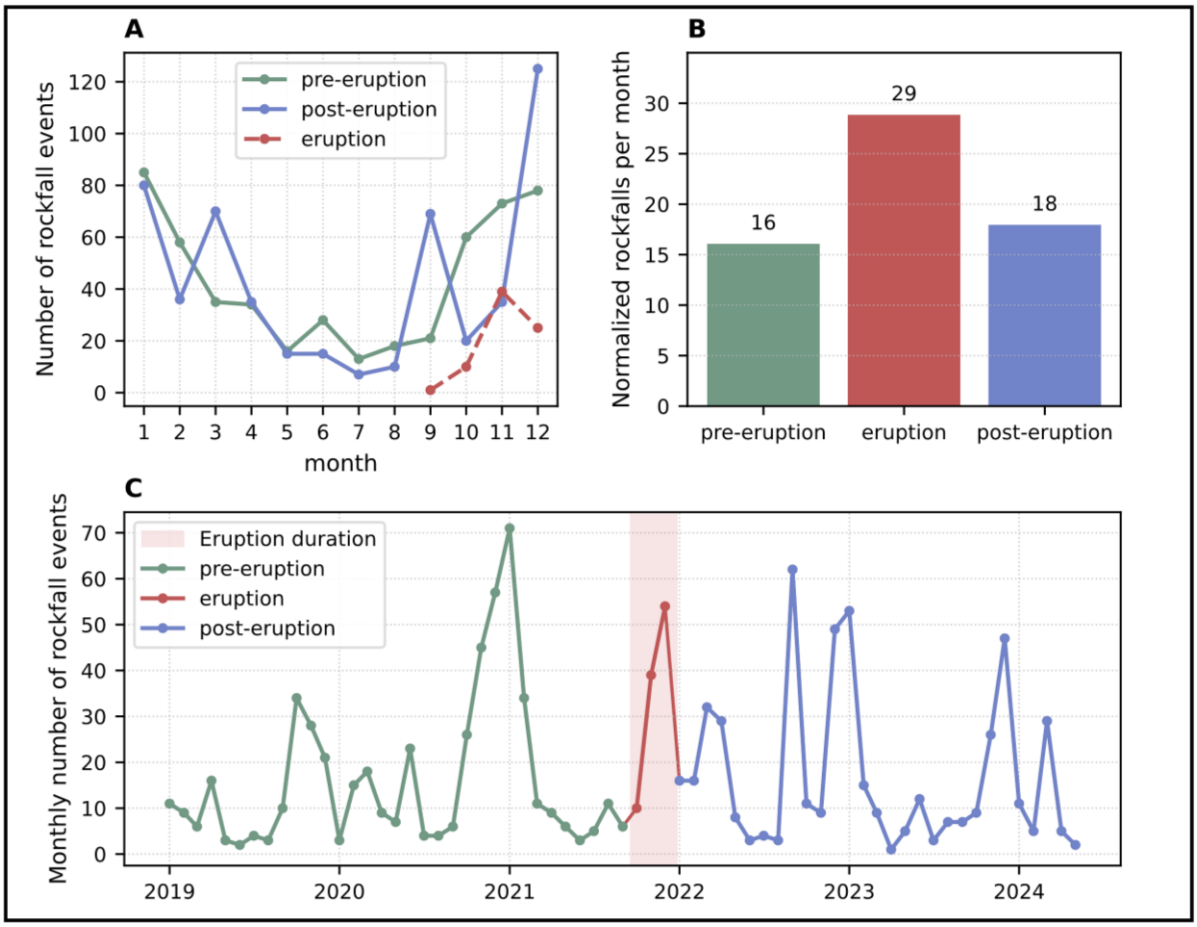

Figure 5. (A) Monthly rockfall counts by study period (eruption period includes only September–December 2021). (B) Normalized rockfalls per month, accounting for period duration. (C) Observed monthly rockfall counts in the study period

The results show a consistent annual pattern in the pre- and post-eruption data, with peaks in December–January and lows during the summer months, particularly July and August. This pattern suggests a seasonal influence on rockfall occurrence, likely associated with rainfall. Although the eruption period covers only September to December, the distribution of rockfalls during this interval appears to follow the typical end-of-year increase, with activity rising in November and December. These observations are consistent with La Palma's climatic regime, in which the rainy season generally spans from October to March, with December being the wettest month, while the summer period from May to August is markedly dry (according to AEMET, the Spanish State Meteorological Agency).

To compare rockfall frequency across periods of unequal duration, total counts were normalized by the number of months in each period (based on calendar days). This produced a standardized rate expressed as the average number of rockfalls per month. The eruption period showed the highest monthly rate (29 rockfalls/month), despite lasting only 2.8 months. In contrast, the pre- and post-eruption periods showed lower rates of 16 and 18 rockfalls per month, respectively. These results indicate a clear increase in rockfall occurrence during the eruption, followed by a moderate decline that remained above the pre-eruption baseline (Figure 5).

Prior to the eruption, monthly rockfall counts remained relatively low, aside from a pronounced peak in late 2020 and early 2021, likely associated with the pre-eruptive seismicity and seasonal rainfall. During the eruption, monthly counts increased but did not exceed the peak observed during the preceding winter. In the post-eruption period, activity remained moderately elevated relative to the pre-eruption baseline and continued to follow a similar seasonal pattern. Over time, however, the magnitude of peak months appears to decrease, suggesting a reduced contribution from seismic forcing compared with the pre-eruption phase (Figure 5).

La Palma shows pronounced climatic contrasts despite its small surface area (708 km²) due to the interaction of steep volcanic topography, persistent northeast trade winds, and a subsidence inversion layer typically located between 600 and 1,500 m a.s.l. [64]. The island rises from sea level to 2,426 m over short horizontal distances, producing strong orographic gradients in temperature and precipitation. On the eastern windward slopes, uplift of moist trade winds generates higher rainfall and frequent fog at mid-elevations, whereas the western leeward flanks remain comparatively dry [65]. In cloud-forest zones on comparable Canary Islands, occult precipitation can contribute up to half of the annual water input, reaching approximately 720 mm yr^{-1} in addition to measured rainfall [66]. La Palma is characterized as environmentally heterogeneous based on 890 sampling plots [67], showing that precipitation, temperature, and cloud frequency vary sharply over short distances. These conditions create spatially variable hydrological regimes that influence rock weathering, pore-water pressure development, and slope stability along road corridors.

Rainfall-triggered rockfalls have previously been documented in the Canary Islands. Statistical analyses conducted on Gran Canaria and Tenerife show a clear seasonal correspondence between monthly rainfall and rockfall occurrence, with peak activity during the wet season (October–March) [68]. In the Anaga massif of Tenerife, a direct relationship between accumulated rainfall and rockfall probability has also been demonstrated, with some failures occurring several days after peak precipitation due to delayed hydro-mechanical responses within steep volcanic slopes [22].

The seasonal increase in rockfall frequency observed in the present dataset during the late autumn and winter months is consistent with this established rainfall control. However, because the rainfall–rockfall relationship has already been documented in the archipelago, the present study does not attempt to derive rainfall thresholds. Instead, the analysis focuses on how volcanic unrest and eruptive activity modified rockfall occurrence relative to this known climatic background.

3.3. Lithological Controls on Rockfall Distribution

The distribution of rockfall events across lithologies (Table 3) shows differences in both absolute frequency and relative contribution over time. Altered basalts consistently account for the largest number of events in all three periods, consistent with their wide spatial distribution (Figure 1) and structural weakness (Table 4). Fresh basalts also contribute a substantial number of events, particularly before the eruption; however, their share declines in the post-eruption period, which may indicate a release of accumulated instability prior to the main eruptive phase.

When event counts are normalized by the total number of events in each period, differences in lithological contribution become clearer. During the eruption, alluvium/colluvium and loose pyroclasts account for a larger proportion of events than in the pre- and post-eruption periods. This pattern is consistent with seismic shaking preferentially triggering failures in unconsolidated and mechanically weak materials [38]. Although altered basalts remain the dominant lithology in absolute numbers, reflecting their wide spatial extent and alteration [17], their proportional contribution decreases during the eruption as activity increases in unconsolidated deposits. Fresh basalts and other mechanically stronger lithologies (Table 4) show the same pattern, with lower proportional representation during the eruption period (Figure 6).

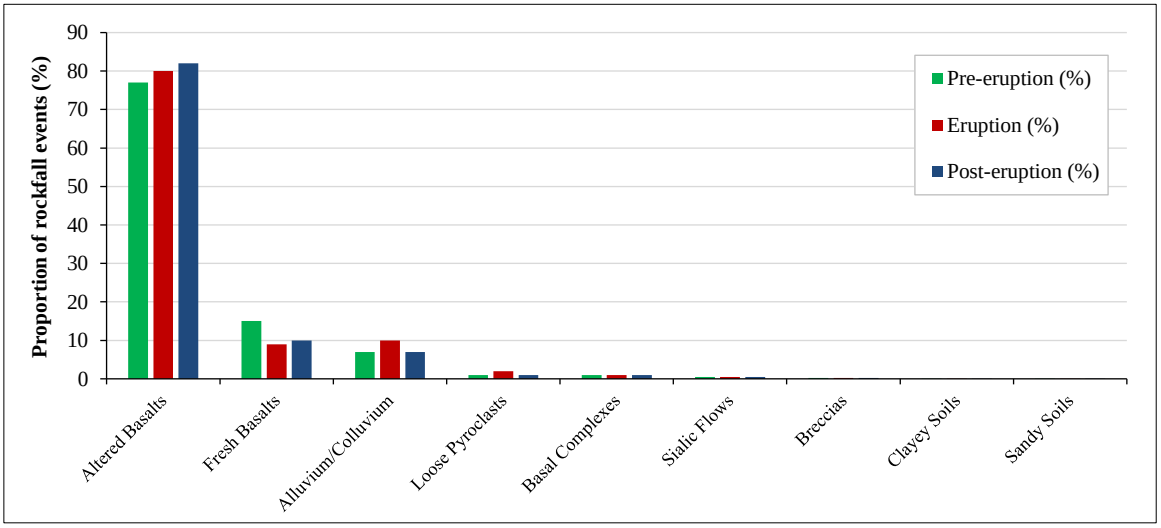

Figure 6. Relative frequency of rockfall events per lithology, normalized within each study period

Among the lithologies with higher event counts, altered basalts show an increase in rockfall activity, rising from 391 events pre-eruption period to 423 in the post-eruption period, corresponding to a 21% relative increase when normalized by period duration. In contrast, fresh basalts show a decrease from 75 to 52 events over the same periods, representing a 22% reduction. These patterns indicate that rockfall activity remained concentrated in more weathered and structurally weakened units, whereas fresher basaltic formations show lower susceptibility to continued detachment following the eruptive phase.

Fresh basalts and basal complex units show a decrease in rockfall occurrence in the post-eruption period, whereas altered basalts show increases. This contrast may reflect differences in mechanical responses of these lithologies to the pre-eruption seismic sequence [69]. In more competent units, such as fresh basalts and the basal complex, pre-eruption shaking may have already mobilized the most unstable material, resulting in fewer subsequent failures. In contrast, the more fractured and altered basalts may have remained susceptible to continued detachment following the seismic build-up, leading to higher post-eruption rockfall activity.

The lithological patterns observed in this study are consistent with previous work highlighting the strong influence of rock mass quality and alteration on rockfall generation in volcanic terrains. Alteration processes, including hydrothermal alteration in volcanic systems can substantially reduce the mechanical strength of volcanic rocks and introduce pronounced spatial heterogeneity in rock strength, thereby promoting slope instability along volcanic flanks and fracture-controlled pathways [38]. Field observations from other road rockfall studies similarly indicate that detached blocks are commonly derived from moderately weathered or altered rock units [17]. More broadly, lithology and rock mass condition exert a strong control on rockfall characteristics, including block size and potential failure volume, with poorer rock mass quality typically producing more frequent detachment [61]. Within this framework, the increased proportion of failures in loose pyroclastic deposits during the eruption likely reflects the susceptibility of unconsolidated volcanic materials to seismic shaking associated with the eruption, whereas the decline in fresh basalt failures after the eruption suggests that the most unstable blocks within these more competent units may have already been mobilized during the pre-eruptive seismic sequence.

- **Rockfall Dynamics in Volcanic Environments**

This study examined whether rockfall occurrence on volcanic islands increases during eruptive phases relative to the periods preceding and following an eruption. Despite the short duration of the Tajogaite eruption (approximately three months), the normalized monthly rate of recorded rockfalls was higher during the eruptive phase than during the pre- and post-eruption periods. This pattern indicates that eruptive conditions were associated with a temporary increase in rockfall activity, consistent with the additional destabilizing influence of eruption-related seismicity and ground deformation acting on already susceptible volcanic slopes [29, 38, 70, 71].

Rockfalls constitute a recurrent geohazard in the Canary Islands and frequently affect transport corridors and nearby settlements, particularly where roads traverse steep volcanic slopes [20, 41, 46]. Previous studies in the region have mainly examined the relationship between rockfall occurrence and rainfall episodes, identifying precipitation as an important triggering factor in volcanic terrains [22, 68]. In parallel, several approaches have been developed to evaluate slope stability and rockfall susceptibility in the archipelago, including methods such as the Volcanic Slope Rating (VSR), which provides a geomechanical framework for assessing instability in volcanic rock masses [72].

In contrast, studies conducted in other volcanic settings, such as Piton de la Fournaise, have largely emphasized the role of rockfalls as potential precursors to eruptions [40]. These studies often analyze the spatial distribution of rockfalls and incorporate additional factors like rainfall to interpret slope instability patterns [33, 73]. In steep volcanic terrains, precipitation is widely recognized as an important trigger, as infiltration and pore-pressure changes can reduce slope stability and promote detachment of fractured rock masses [9, 24, 68, 74].

Across previous case studies, rockfall activity has been observed to increase during periods approaching eruptive events [25]. Such increases are commonly interpreted as a response to growing slope instability and repeated ground shaking associated with pre-eruptive seismic swarms [69]. Several mechanisms may explain the temporal patterns observed in this study. Seismic shaking associated with magma migration and eruptive activity can destabilize fractured rock masses and trigger detachment on steep slopes. Ground motion promotes the opening of existing joints, reduces the mechanical equilibrium of blocks, and can initiate rockfalls, wedge failures, and movements within talus or scree deposits. Similar seismogeological effects have been documented in earthquake-affected regions, where shaking produced joint opening, block splitting, and various forms of slope failure ranging from individual rockfalls to larger mass movements [70]. Within volcanic settings, repeated low-magnitude seismic events may progressively weaken already fractured rock masses, increasing the likelihood of detachment during periods of volcanic unrest.

Slope destabilization may also evolve over longer timescales. Post-seismic studies show that landslides and rockfalls frequently persist after the main triggering event, reflecting delayed geomorphic responses and the gradual

remobilization of unstable material [71]. In some regions, cascading slope hazards have continued for years or even decades following major earthquakes, driven by the reactivation of previously destabilized slopes and the progressive release of accumulated instability [75]. These delayed responses suggest that seismic disturbances may initiate a phase of prolonged slope adjustment rather than producing only immediate failures. In the context of La Palma, the elevated proportion of higher-severity events during and after the eruption may partly reflect this progressive destabilization of slopes subjected to repeated seismic forcing [29, 76].

Volcanic slope instability is not restricted to eruptive phases. Instability has been documented during quiescent periods in several volcanic systems, particularly where degassing and hydrothermal alteration weaken rock masses over time [38]. These internal volcanic processes can progressively modify rock strength and fracture networks, increasing susceptibility to slope failure even in the absence of eruptive activity. This perspective is consistent with the persistent background level of rockfall activity observed in the La Palma dataset, where events occurred throughout the study period regardless of eruptive conditions.

Rockfall occurrence is difficult to quantify despite being one of the dominant geomorphic processes shaping steep rock slopes. The episodic nature of rockfalls and the absence of systematic monitoring mean that reliable long-term inventories are rarely available, limiting the ability to analyze temporal patterns and triggering mechanisms [77]. In many regions, rockfall hazard studies remain constrained by the lack of historical occurrence data, which restricts both statistical analysis and the evaluation of slope instability processes [15]. More broadly, rockfall analysis requires detailed information on slope geometry, geological structure, lithology, meteorological conditions, and land cover, data that are seldom available simultaneously, introducing significant uncertainty into hazard assessments [61, 78].

For this reason, operational incident databases maintained by infrastructure or emergency agencies provide an important empirical source of information. Such records typically document the timing and location of events together with qualitative descriptions of falling material and infrastructure impacts, including road obstruction, vehicle damage, or traffic disruption [74]. Although these datasets rarely include precise measurements of block volume, descriptors of block size or roadway obstruction can provide useful proxies for event magnitude, a key parameter in rockfall hazard analysis [2, 79]. Similar maintenance records have been used to reconstruct long-term rockfall activity along transportation corridors, such as multi-decade inventories of rock slope failures affecting highways and railways in British Columbia [63]. In this context, the CECOPIN database used in this study represents a rare multi-year inventory of road-related rockfall incidents on La Palma. By systematically coding operational descriptors into standardized event categories and an ordinal severity scale, the dataset provides a structured basis for analysing the temporal behaviour of rockfall activity and its relationship with eruptive and lithological controls.

Several limitations should be acknowledged. The dataset is derived from operational reports and therefore records rockfalls that affected roads or accessible infrastructure rather than the full range of slope failures occurring across the island. This reflects the structural configuration of La Palma's road network, where transport corridors are commonly excavated directly into steep volcanic slopes and therefore represent the principal interface between slope instability and human activity. Consequently, the database documents rockfalls in their hazard dimension, that is, where slope failure interacts with infrastructure and requires operational response. At the same time, operational reporting introduces unavoidable biases, including possible underreporting of minor events, higher reporting probability along trafficked roads, and the absence of direct measurements of block volume or failure geometry. These constraints are inherent to incident-based inventories and are acknowledged within the scope of the analysis.

Rockfalls represent a particularly relevant hazard on La Palma due to the island's steep volcanic relief, narrow and low-redundancy road network, and high levels of tourism. Many transport routes and recreational paths traverse steep slopes where rockfalls can directly affect mobility and visitor safety [41]. In mountainous areas, tourists are often the main elements at risk, and their presence varies strongly in time and space, which can substantially influence exposure to rockfall hazards [61]. On an island that remains volcanically active and heavily visited, understanding how eruptive and seismic processes influence rockfall occurrence is therefore essential for assessing infrastructure vulnerability and managing risk along frequently used road corridors and tourist routes.

From a risk-management perspective, these findings underline the importance of mitigation measures along volcanic road corridors. Engineering approaches such as catchment ditches, rock reinforcement, wire mesh systems, protective barriers, and slope regrading are commonly applied to reduce rockfall risk in steep terrain. For example, numerical analyses of volcanic slope geometries have been used to optimize catch ditch design and estimate block stop distances under different material and slope conditions, providing practical design criteria for road infrastructure in volcanic environments [80]. Integrating geological susceptibility assessments with such mitigation strategies is therefore essential for reducing the impacts of rockfalls on transport networks in volcanic islands.

4. Conclusion

This study statistically analyzed the temporal evolution of road-related rockfalls on La Palma (Canary Islands, Spain) in relation to the 2021 Tajogaite eruption, using a multi-year incident dataset to compare rockfall occurrence, severity, and lithological distribution across the pre-eruption, eruption, and post-eruption periods. Rockfall dynamics on volcanic islands such as La Palma reflect the combined influence of lithological susceptibility, structural conditions, and external triggering processes, including rainfall and seismic activity. The analysis indicates that the total number of recorded events remained nearly identical before and after the 2021 Tajogaite eruption, pointing to a persistent baseline level of slope instability. This pattern suggests that rockfall occurrence on the island is not limited to eruptive episodes but is strongly conditioned by pre-existing geological weaknesses and ongoing slope processes, with eruptive or seismic disturbances acting primarily as episodic triggers rather than the dominant control on long-term activity.

During the eruption, both the relative severity and the normalized rate of rockfall occurrence increased. The proportion of high-severity events (severity levels 4 and 5 in the classification used in this study) rose significantly compared with the pre-eruption baseline, as supported by statistical testing. This pattern indicates that eruptive conditions were associated with a higher likelihood of larger rockfalls affecting the road network, consistent with the destabilizing influence of eruption-related seismic activity on fractured volcanic slopes.

Lithological characteristics further influenced these patterns. Altered basalts, characterized by structural weakening and weathering, consistently recorded the highest number of events across all periods. In contrast, fresh basalts and other more competent units showed reduced activity in the post-eruption period, suggesting that earlier seismic shaking may have already mobilized the most unstable material in these lithologies. Normalized distributions also indicate that unconsolidated units, particularly pyroclastic deposits and alluvium, became proportionally more active during the eruption, highlighting the role of material properties in controlling slope response to seismic forcing.

Although eruptive activity can intensify slope instability, rockfall occurrence in the Canary Islands is not limited to eruptive phases. The recorded events before the eruption indicate that rockfalls are part of the island's persistent slope dynamics. The elevated activity observed prior to the eruption is consistent with the documented increase in pre-eruptive seismicity, highlighting the importance of considering both eruptive and pre-eruptive processes in rockfall monitoring and hazard assessment.

These findings indicate that the timing of seismic activity relative to eruptive processes, together with lithological susceptibility, influences both the occurrence and severity of rockfall hazards. Effective risk mitigation on volcanic islands therefore requires the integration of geological susceptibility assessments, seismic monitoring, and continued post-eruption surveillance to manage both immediate and longer-term impacts on exposed infrastructure and populated areas.

5. Declarations

5.1. Author Contributions

Conceptualization, J.C.S., L.E.H.G., and S.L.; methodology, J.K. and J.C.S.; software, J.K. and M.H.; validation, J.C.S., N.C.P., L.E.H.G., and S.L.; formal analysis, J.K. and N.C.P.; investigation, J.K. and M.H.; resources, R.G.M. and J.C.S.; data curation, R.G.M. and J.K.; writing—original draft preparation, J.K., N.C.P., and M.H.; writing—review and editing, J.C.S., L.E.H.G., and S.L.; visualization, J.K.; supervision, J.C.S. and L.E.H.G.; project administration, J.C.S.; funding acquisition, J.C.S. All authors have read and agreed to the published version of the manuscript.

5.2. Data Availability Statement

Data was obtained from Centro de Coordinación Operativa Insular of La Palma and are available from the corresponding author on reasonable request with the permission of CECOPIN.

5.3. Funding and Acknowledgments

This research was partially supported by the HORIZON-MISS-2023-CLIMA-01-02 programme through the project Geologically Enhanced NaturE-based Solutions for Climate Change Resiliency of Critical Water Infrastructure (GENESIS), Grant Agreement No. 101157447. The authors would also like to thank CECOPIN for providing the rockfall data from the period 2019-2024, which enabled the assessment of the eruption's impact on these findings.

5.4. Conflicts of Interest

The authors declare no conflict of interest.

6. References

[1] Hantz, D., Vengeon, J. M., & Dussauge-Peisser, C. (2003). An historical, geomechanical and probabilistic approach to rock-fall hazard assessment. Natural Hazards and Earth System Science, 3(6), 693–701. doi:10.5194/nhess-3-693-2003.

[2] Ferrari, F., Giacomini, A., & Thoeni, K. (2016). Qualitative Rockfall Hazard Assessment: A Comprehensive Review of Current Practices. Rock Mechanics and Rock Engineering, 49(7), 2865–2922. doi:10.1007/s00603-016-0918-z.

[3] Ayonghe, S. N., Mafany, G. T., Ntasin, E., & Samalang, P. (1999). Seismically activated swarm of landslides, tension cracks, and a rockfall after heavy rainfall in Bafaka, Cameroon. Natural Hazards, 19(1), 13–27. doi:10.1023/A:1008041205256.

[4] Dang, D., Gong, L., Jin, C., Qin, J., Yang, T., & Jia, Z. (2025). Risk evaluation of rockfall hazard in the tunnel portals of western mountain railway tunnels based on the improved G1–EWM–UMT model. Natural Hazards, 121(12), 14373–14398. doi:10.1007/s11069-025-07359-0.

[5] Siddique, T., Pradhan, S.P. (2025). Rockfall Hazard Assessment and Mitigation Strategies Along NH-7, Garhwal Himalaya: An Integrated RHRS and Numerical Simulation Approach. The Himalaya Dilemma, Springer Natural Hazards, Springer, Cham, Switzerland. doi:10.1007/978-3-031-95083-4_8.

[6] UNDRR. (2007). Definition: Hazard. United Nations Office for Disaster Risk Reduction (UNDRR), Geneva, Switzerland. Available online: https://www.undrr.org/terminology/hazard (accessed on April 2026).

[7] Shen, G., Zhou, L., Wu, Y., & Cai, Z. (2018). A global expected risk analysis of fatalities, injuries, and damages by natural disasters. Sustainability (Switzerland), 10(7), 2573. doi:10.3390/su10072573.

[8] Maheshwari, S., Bhowmik, R., & Samanta, M. (2025). Mechanics and modelling approaches of rockfall: a comprehensive review for hazard mitigation in hill roads. Arabian Journal of Geosciences, 18(2), 45. doi:10.1007/s12517-025-12189-2.

[9] Goli Mokhtari, L. (2026). Optimizing graph neural networks for rockfall susceptibility mapping: a feature selection and hazard prediction approach. Natural Hazards, 122(1), 20. doi:10.1007/s11069-025-07855-3.

[10] Rosly, M. H., Mohamad, H. M., Bolong, N., & Harith, N. S. H. (2023). Relationship of Rainfall Intensity with Slope Stability. Civil Engineering Journal, 9, 75–82. doi:10.28991/CEJ-SP2023-09-06.

[11] Fanos, A. M., & Pradhan, B. (2016). Multi-scenario Rockfall Hazard Assessment Using LiDAR Data and GIS. Geotechnical and Geological Engineering, 34(5), 1375–1393. doi:10.1007/s10706-016-0049-z.

[12] Cignetti, M., Godone, D., Bertolo, D., Paganone, M., Thuegaz, P., & Giordan, D. (2021). Rockfall susceptibility along the regional road network of Aosta Valley Region (northwestern Italy). Journal of Maps, 17(3), 54–64. doi:10.1080/17445647.2020.1850534.

[13] Wahlen, S., Meier, L., & Darms, G. (2020). Rockfall Alarm System with Automatic Road Closure/Reopening and long-term Slope Monitoring for major European North-South Route (Axenstrasse). EGU General Assembly Conference Abstracts, 4-8 May, 2020. doi:10.5194/egusphere-egu2020-5138.

[14] Farvacque, M., Lopez-Saez, J., Corona, C., Toe, D., Bourrier, F., & Eckert, N. (2019). How is rockfall risk impacted by land-use and land-cover changes? Insights from the French Alps. Global and Planetary Change, 174, 138–152. doi:10.1016/j.gloplacha.2019.01.009.

[15] Dahiya, N., Pandit, K., Sarkar, S., & Pain, A. (2025). Various Aspects of Rockfall Hazards along the Mountain Roads in India: a Systematic Review. Indian Geotechnical Journal, 55(3), 2007–2029. doi:10.1007/s40098-024-01015-3.

[16] Pandey, V. H. R., Kushwaha, G., Kainthola, A., Yadav, V., Singh, T. N., & Krishna, A. S. (2025). Field data driven rockfall hazard and risk assessment along Sangla-Chitkul road, Himachal Pradesh, India. Bulletin of Engineering Geology and the Environment, 84(6), 329. doi:10.1007/s10064-025-04286-z.

[17] Ahmad, M., Umrao, R. K., Ansari, M. K., Singh, R., & Singh, T. N. (2013). Assessment of Rockfall Hazard along the Road Cut Slopes of State Highway-72, Maharashtra, India. Geomaterials, 3(1), 15–23. doi:10.4236/gm.2013.31002.

[18] Jordá-Bordehore, L., Albán, L. G., Valenzuela, R. C., Bravo, G., Menoscal-Menoscal, M., Larreta, E., Garces, D., & Mulas, M. (2023). An Analysis of Slope Stability in the Penipe–Baños Road by Applying Empirical Methods, Kinematic Analysis and Remote Photogrammetry Techniques. Geosciences (Switzerland), 13(12), 366. doi:10.3390/geosciences13120366.

[19] Voumard, J., Baumann, V., Jaboyedoff, M., Derron, M. H., & Penna, I. (2014). Risk assessment on an Argentinean road with a dynamic traffic simulator. EGU General Assembly Conference, 27 April-2 May, 2014, Vienna, Austria.

[20] Galindo, I., Montoya-Montes, I., García López-Davalillo, J. C., Sarro, R., Llorente, M., Sánchez, N., Santamarta, J. C., Cruz-Pérez, N., Ortega, A., & Mateos, R. M. (2023). Identification and Management of Indirect Volcanic Risks: Citizens' Rockfall Observatory on the Island of El Hierro. El Hierro Island, Active Volcanoes of the World, Springer, Cham, Switzerland. doi:10.1007/978-3-031-35135-8_12.

[21] Volkwein, A., Schellenberg, K., Labiouse, V., Agliardi, F., Berger, F., Bourrier, F., Dorren, L. K. A., Gerber, W., & Jaboyedoff, M. (2011). Rockfall characterisation and structural protection - A review. Natural Hazards and Earth System Science, 11(9), 2617–2651. doi:10.5194/nhess-11-2617-2011.

[22] Leyva, S., Cruz-Pérez, N., Rodríguez-Martín, J., Miklin, L., & Santamarta, J. C. (2022). Rockfall and Rainfall Correlation in the Anaga Nature Reserve in Tenerife (Canary Islands, Spain). Rock Mechanics and Rock Engineering, 55(4), 2173–2181. doi:10.1007/s00603-021-02762-y.

[23] Dorren, L. K. A. (2003). A review of rockfall mechanics and modelling approaches. Progress in Physical Geography, 27(1), 69–87. doi:10.1191/0309133303pp359ra.

[24] Wieczorek, G. F., & Jäger, S. (1996). Triggering mechanisms and depositional rates of postglacial slope-movement processes in the Yosemite Valley, California. Geomorphology, 15(1), 17–31. doi:10.1016/0169-555X(95)00112-I.

[25] Hibert, C., Mangeney, A., Grandjean, G., Peltier, A., DiMuro, A., Shapiro, N. M., Ferrazzini, V., Boissier, P., Durand, V., & Kowalski, P. (2017). Spatio-temporal evolution of rockfall activity from 2007 to 2011 at the Piton de la Fournaise volcano inferred from seismic data. Journal of Volcanology and Geothermal Research, 333–334, 36–52. doi:10.1016/j.jvolgeores.2017.01.007.

[26] Jaboyedoff, M., Baillifard, F., Bardou, E., & Girod, F. (2004). The effect of weathering on Alpine rock instability. Quarterly Journal of Engineering Geology and Hydrogeology, 37(2), 95–103. doi:10.1144/1470-9236/03-046.

[27] Zhang, Y., Zhang, J., Chen, G., Zheng, L., & Li, Y. (2015). Effects of vertical seismic force on initiation of the Daguangbao landslide induced by the 2008 Wenchuan earthquake. Soil Dynamics and Earthquake Engineering, 73, 91–102. doi:10.1016/j.soildyn.2014.06.036.

[28] Hung, C., Liu, C. H., Lin, G. W., & Leshchinsky, B. (2019). The Aso-Bridge coseismic landslide: a numerical investigation of failure and runout behavior using finite and discrete element methods. Bulletin of Engineering Geology and the Environment, 78(4), 2459–2472. doi:10.1007/s10064-018-1309-3.

[29] Nasir, N. F., Mohamad, H. M., Haziq Rosly, M., Omar, H. A., & Hamansa, H. (2025). Quantifying Slope Stability and Landslide Susceptibility Through Rainfall-Induced Geotechnical Assessment. Civil Engineering Journal, 11(12), 5226–5237. doi:10.28991/CEJ-2025-011-12-017.

[30] Li, X.-n., Ling, S.-x., Sun, C.-w., Xu, J.-x., & Huang, T. (2019). Integrated rockfall hazard and risk assessment along highways: An example for Jiuzhaigou area after the 2017 Ms 7.0 Jiuzhaigou earthquake, China. Journal of Mountain Science, 16(6), 1318–1335. doi:10.1007/s11629-018-5355-x.

[31] Piattelli, V., Cinosi, J., Paglia, G., Mancinelli, V., Esposito, G., & Miccadei, E. (2025). Geomorphological Analysis, Rockfall Susceptibility, and Preliminary Hazard Assessment: Case Studies From the Abruzzo Region (Central Italy). Earth Systems and Environment, 9(4), 3207–3230. doi:10.1007/s41748-024-00545-3.

[32] Zhao, E., Wen, J., Bai, X., Han, Q., & Du, X. (2026). A joint probability model for multi-hazard intensity in earthquake-induced rockfall scenarios. Reliability Engineering & System Safety, 273, 112342. doi:10.1016/j.ress.2026.112342.

[33] Durand, V., Mangeney, A., Haas, F., Jia, X., Bonilla, F., Peltier, A., Hibert, C., Ferrazzini, V., Kowalski, P., Lauret, F., Brunet, C., Satriano, C., Wegner, K., Delorme, A., & Villeneuve, N. (2018). On the Link Between External Forcings and Slope Instabilities in the Piton de la Fournaise Summit Crater, Reunion Island. Journal of Geophysical Research: Earth Surface, 123(10), 2422–2442. doi:10.1029/2017JF004507.

[34] Durand, V., Mangeney, A., Bernard, P., Jia, X., Bonilla, F., Satriano, C., Saurel, J. M., Aissaoui, E. M., Peltier, A., Ferrazzini, V., Kowalski, P., Lauret, F., Brunet, C., & Hibert, C. (2023). Repetitive small seismicity coupled with rainfall can trigger large slope instabilities on metastable volcanic edifices. Communications Earth and Environment, 4(1), 383. doi:10.1038/s43247-023-00996-y.

[35] Zobin, V. M., Navarro, C., & Tellez, A. (2021). Insight into lava dome extrusion dynamics from seismic signatures of pyroclastic flows and incandescent rockfalls: Volcán de Colima, México, 1998–2017. Bulletin of Volcanology, 83(7), 44. doi:10.1007/s00445-021-01463-2.

[36] Calder, E. S., Cortés, J. A., Palma, J. L., & Luckett, R. (2005). Probabilistic analysis of rockfall frequencies during an andesite lava dome eruption: The Soufrière Hills Volcano, Montserrat. Geophysical Research Letters, 32(16). doi:10.1029/2005GL023594.

[37] de Vallejo, L. I. G., Hernández-Gutiérrez, L. E., Miranda, A., & Ferrer, M. (2020). Rockfall hazard assessment in volcanic regions T. Geosciences (Switzerland), 10(6), 1–20. doi:10.3390/geosciences10060220.

[38] De Jarnatt, B. F., Walter, T. R., Heap, M. J., Müller, D., & Pisciotta, A. F. (2026). Hydrothermal weakening and slope instability at Vulcano (Italy) analyzed using drones and in-situ strength measurements. Communications Earth and Environment, 7(1), 3. doi:10.1038/s43247-025-03014-5.

[39] Poganj, A., Heap, M. J., & Baud, P. (2025). Spatial distribution of alteration and strength in a lava dome: Implications for large-scale volcano stability modelling. Journal of Volcanology and Geothermal Research, 463, 108344. doi:10.1016/j.jvolgeores.2025.108344.

[40] Battaglia, J. (2003). Location of seismic events and eruptive fissures on the Piton de la Fournaise volcano using seismic amplitudes. Journal of Geophysical Research, 108(B8), 1-14. doi:10.1029/2002jb002193.

[41] Montoya-Montes, I., Galindo, I., Sánchez, N., López-Davalillo, J. C. G., García, I., Pérez, N. C., Ortega, A., Santamarta, J. C., Rodríguez Alcántara, J. S., Hernández Ruiz, M., Sanabria Pabón, M., Lorenzo Carnicero, C., Sarro, R., & Mateos, R. M. (2025). Citizens' Observatory on Rockfalls in the Canary Islands, Spain. Citizens' Observatories on Geohazards. Geoenvironmental Disaster Reduction, Springer, Cham, Switzerland. doi:10.1007/978-3-031-53371-6_9.

[42] PEIN TENERIFE. (2020). Chapter III: Risk Analysis Island Territorial Emergency Plan for Civil Protection of the Island of Tenerife: Risk Classification. Island Directorate of Security, Area of Sustainability, Environment and Security, Island Emergency Plan (PEIN), Spain. Available online: https://transparencia.tenerife.es/archivos/110/documento-plan-39-16-03-2020-analisis-de-riesgos-capitulo-3-3738.pdf (accessed on April 2026).

[43] Ortega Rodriguez, A., Carrilho Gomes, R., Telmo Jeremias, F., Santamarta Cerezal, J. C., Quental, L., Galindo Jiménez, I., ... & O'Hare, G. (2020). AGEO-Natural hazard prevention and awareness raising through citizen observatories. EGU General Assembly Conference, Session HS1.2.4. doi:10.5194/egusphere-egu2020-13519.

[44] Cruz-Pérez, N., Rodríguez-Martín, J., Galindo, I., Montoya, I., Sánchez, N., Hernández-Gutiérrez, L. E., Ortega Rodríguez, A., Leyva, S., & Santamarta, J. C. (2021). Citizen Observatories Applied To Geological Risk Management. INTED2021 Proceedings, 1, 1022–1025. doi:10.21125/inted.2021.0250.

[45] Sarro, R., María Mateos, R., Reichenbach, P., Aguilera, H., Riquelme, A., Hernández-Gutiérrez, L. E., Martín, A., Barra, A., Solari, L., Monserrat, O., Alvioli, M., Fernández-Merodo, J. A., López-Vinielles, J., & Herrera, G. (2020). Geotechnics for rockfall assessment in the volcanic island of Gran Canaria (Canary Islands, Spain). Journal of Maps, 16(2), 605–613. doi:10.1080/17445647.2020.1806125.

[46] Sarro, R., Rossi, M., Reichenbach, P., & Mateos, R. M. (2025). From rockfall source area identification to susceptibility zonation: a proposed workflow tested on El Hierro (Canary Islands, Spain). Natural Hazards and Earth System Sciences, 25(4), 1459–1479. doi:10.5194/nhess-25-1459-2025.

[47] Rossi, M., Sarro, R., Reichenbach, P., & Mateos, R. M. (2021). Probabilistic identification of rockfall source areas at regional scale in El Hierro (Canary Islands, Spain). Geomorphology, 381, 107661. doi:10.1016/j.geomorph.2021.107661.

[48] Dominguez, L., Biass, S., Frischknecht, C., Weir, A., Reyes-Hardy, M.-P., Di Maio, L. S., Pérez, N., & Bonadonna, C. (2025). Quantifying cascading impacts through road network analysis in an insular volcanic setting: the 2021 Tajogaite eruption of La Palma Island (Spain). Natural Hazards and Earth System Sciences, 25(12), 4815–4841. doi:10.5194/nhess-25-4815-2025.

[49] Žabota, B., & Kobal, M. (2018). Overview of used rockfall modeling methods in Slovenia. Gozdarski Vestnik (Forestry Journal), 76(2), 55-71.

[50] Romero, J. E., Burton, M., Cáceres, F., Taddeucci, J., Civico, R., Ricci, T., Pankhurst, M. J., Hernández, P. A., Bonadonna, C., Llewellin, E. W., Pistolesi, M., Polacci, M., Solana, C., D'Auria, L., Arzilli, F., Andronico, D., Rodríguez, F., Asensio-Ramos, M., Martín-Lorenzo, A., … Perez, N. M. (2022). The initial phase of the 2021 Cumbre Vieja ridge eruption (Canary Islands): Products and dynamics controlling edifice growth and collapse. Journal of Volcanology and Geothermal Research, 431, 107642. doi:10.1016/j.jvolgeores.2022.107642.

[51] Bonadonna, C., Pistolesi, M., Biass, S., Voloschina, M., Romero, J., Coppola, D., Folch, A., D'Auria, L., Martin-Lorenzo, A., Dominguez, L., Pastore, C., Reyes Hardy, M. P., & Rodríguez, F. (2022). Physical Characterization of Long-Lasting Hybrid Eruptions: The 2021 Tajogaite Eruption of Cumbre Vieja (La Palma, Canary Islands). Journal of Geophysical Research: Solid Earth, 127(11), 2022 025302. doi:10.1029/2022JB025302.

[52] Filonchyk, M., Peterson, M. P., Gusev, A., Hu, F., Yan, H., & Zhou, L. (2022). Measuring air pollution from the 2021 Canary Islands volcanic eruption. Science of the Total Environment, 849, 157827. doi:10.1016/j.scitotenv.2022.157827.

[53] Tashima, M. M., Soriano, L., Borrachero, M. V., Monzó, J., & Payá, J. (2023). Towards the valorization of Cumbre Vieja volcanic ash – Production of alternative cements. Construction and Building Materials, 370, 130635. doi:10.1016/j.conbuildmat.2023.130635.

[54] Escolà-Gascón, Á., Dagnall, N., Denovan, A., Diez-Bosch, M., & Micó-Sanz, J. L. (2023). Social impact of environmental disasters: Evidence from Canary Islands volcanic eruption. International Journal of Disaster Risk Reduction, 88, 103613. doi:10.1016/j.ijdrr.2023.103613.

[55] Ruggieri, F., Forte, G., Bocca, B., Casentini, B., Bruna Petrangeli, A., Salatino, A., & Gimeno, D. (2023). Potentially harmful elements released by volcanic ash of the 2021 Tajogaite eruption (Cumbre Vieja, La Palma Island, Spain): Implications for human health. The Science of the Total Environment, 905, 167103. doi:10.1016/j.scitotenv.2023.167103.

[56] Leoni, V., & Boto-García, D. (2023). The Effect of Natural Disasters on Hotel Demand, Supply and Labour Markets: Evidence from the La Palma Volcano Eruption. Environmental and Resource Economics, 86(4), 755-780. doi:10.1007/s10640-023-00811-4.

[57] Troll, V. R., Aulinas, M., Carracedo, J. C., Geiger, H., Perez-Torrado, F. J., Soler, V., Deegan, F. M., Bloszies, C., Weis, F., Albert, H., Gisbert, G., Day, J. M. D., Rodríguez-Gonzalez, A., Gazel, E., & Dayton, K. (2024). The 2021 La Palma eruption: social dilemmas resulting from life close to an active volcano. Geology Today, 40(3), 96–111. doi:10.1111/gto.12472.

[58] Jiménez, J., Gasco Cavero, S., Marazuela, M. Á., Baquedano, C., Laspidou, C., Santamarta, J. C., & García-Gil, A. (2024). Effects of the 2021 La Palma volcanic eruption on groundwater hydrochemistry: Geochemical modelling of endogenous CO2 release to surface reservoirs, water-rock interaction and influence of thermal and seawater. Science of the Total Environment, 929, 172594. doi:10.1016/j.scitotenv.2024.172594.

[59] Koritnik, J., Cruz-Pérez, N., García-Gil, A., & Santamarta, J. C. (2025). Impacts of the 2021 La Palma volcanic eruption on drinking water quality (Canary Islands, Spain). Natural Hazards, 121(18), 22151–22182. doi:10.1007/s11069-025-07682-6.

[60] Guzzetti, F., Reichenbach, P., Ardizzone, F., Cardinali, M., & Galli, M. (2006). Estimating the quality of landslide susceptibility models. Geomorphology, 81(1–2), 166–184. doi:10.1016/j.geomorph.2006.04.007.

[61] Wang, X., Frattini, P., Stead, D., Sun, J., Liu, H., Valagussa, A., & Li, L. (2020). Dynamic rockfall risk analysis. Engineering Geology, 272, 105622. doi:10.1016/j.enggeo.2020.105622.

[62] Mineo, S. (2020). Comparing rockfall hazard and risk assessment procedures along roads for different planning purposes. Journal of Mountain Science, 17(3), 653–669. doi:10.1007/s11629-019-5766-3.

[63] Hungr, O., Evans, S. G., & Hazzard, J. (1999). Magnitude and frequency of rock falls and rock slides along the main transportation corridors of southwestern British Columbia. Canadian Geotechnical Journal, 36(2), 224–238. doi:10.1139/t98-106.

[64] Gaug, M., Longo, A., Bianchi, S., Font, L., Almirante, S., Kornmayer, H., Doro, M., Hahn, A., Blanch, O., Plastino, W., & Dorner, D. (2024). Detailed analysis of local climate at the CTAO-North site on la Palma from 20 yr of MAGIC weather station data. Monthly Notices of the Royal Astronomical Society, 534(3), 2344–2377. doi:10.1093/mnras/stae2214.

[65] Rodríguez Hernández, D. (2015). Analysis of the thermal gradient on the eastern and western slopes of the Island of La Palma. Final Degree Project, Repositorio Institucional de la Universidad de La Laguna, Spain. Available online: https://riull.ull.es/xmlui/handle/915/1229 (accessed on April 2026).

[66] García-Santos, G., Marzol, M. V., & Aschan, G. (2004). Water dynamics in a laurel montane cloud forest in the Garajonay National Park (Canary Islands, Spain). Hydrology and Earth System Sciences, 8(6), 1065–1075. doi:10.5194/hess-8-1065-2004.

[67] Irl, S. D. H., Harter, D. E. V., Steinbauer, M. J., Gallego Puyol, D., Fernández-Palacios, J. M., Jentsch, A., & Beierkuhnlein, C. (2015). Climate vs. topography - spatial patterns of plant species diversity and endemism on a high-elevation island. Journal of Ecology, 103(6), 1621–1633. doi:10.1111/1365-2745.12463.

[68] Melillo, M., Gariano, S. L., Peruccacci, S., Sarro, R., Mateos, R. M., & Brunetti, M. T. (2020). Rainfall and rockfalls in the Canary Islands: Assessing a seasonal link. Natural Hazards and Earth System Sciences, 20(8), 2307–2317. doi:10.5194/nhess-20-2307-2020.

[69] Suarez, E. D., Domínguez-Cerdeña, I., Villaseñor, A., Aparicio, S. S. M., del Fresno, C., & García-Cañada, L. (2023). Unveiling the pre-eruptive seismic series of the La Palma 2021 eruption: Insights through a fully automated analysis. Journal of Volcanology and Geothermal Research, 444, 107946. doi:10.1016/j.jvolgeores.2023.107946.

[70] Vidrih, R., Ribičič, M., & Suhadolc, P. (2001). Seismogeological effects on rocks during the 12 April 1998 upper Soča territory earthquake (NW Slovenia). Tectonophysics, 330(3–4), 153–175. doi:10.1016/S0040-1951(00)00219-5.

[71] Xu, Q., Fan, X., & Yunus, A. P. (2022). Post-earthquake Landscape Response. Coseismic Landslides. Springer Natural Hazards. Springer, Singapore. doi:10.1007/978-981-19-6597-5_13. doi:10.1007/978-981-19-6597-5_13.

[72] Leyva, S., Cruz-Pérez, N., & Santamarta, J. C. (2024). Refinement of the volcanic slope rating approach for determining slope stability in volcanic rocks of the Canary Islands. Earth Surface Processes and Landforms, 49(15), 5133–5145. doi:10.1002/esp.6022.

[73] DeRoin, N., & McNutt, S. R. (2012). Rockfalls at Augustine Volcano, Alaska: The influence of eruption precursors and seasonal factors on occurrence patterns 1997-2009. Journal of Volcanology and Geothermal Research, 211–212, 61–75. doi:10.1016/j.jvolgeores.2011.11.003.

[74] Ferlisi, S., Cascini, L., Corominas, J., & Matano, F. (2012). Rockfall risk assessment to persons travelling in vehicles along a road: The case study of the Amalfi coastal road (southern Italy). Natural Hazards, 62(2), 691-721. doi:10.1007/s11069-012-0102-z.

[75] Jones, K. E., Howarth, J. D., Massey, C. I., Luković, B., Sirguey, P., Singeisen, C., Gasston, C., Morgenstern, R., & Ries, W. (2025). An alternative to landslide volume-area scaling relationships: an ensemble approach adopting a difference model to estimate the total volume of landsliding triggered by the 2016 Kaikōura earthquake, New Zealand. Landslides, 22(7), 2219–2236. doi:10.1007/s10346-025-02479-x.

[76] Gracchi, T., Lotti, A., Saccorotti, G., Lombardi, L., Nocentini, M., Mugnai, F., Gigli, G., Barla, M., Giorgetti, A., Antolini, F., Fiaschi, A., Matassoni, L., & Casagli, N. (2017). A method for locating rockfall impacts using signals recorded by a microseismic network. Geoenvironmental Disasters, 4(1), 26. doi:10.1186/s40677-017-0091-z.

[77] Duarte, R. M., & Marquínez, J. (2002). The influence of environmental and lithologic factors on rockfall at a regional scale: An evaluation using GIS. Geomorphology, 43(1–2), 117–136. doi:10.1016/S0169-555X(01)00126-X.

[78] Marchelli, M., De Biagi, V., Paganone, M., & Bertolo, D. (2025). A hybrid approach to quantifying rockfall risk with limited knowledge: a case study in Aosta Valley. Bulletin of Engineering Geology and the Environment, 84(11), 471. doi:10.1007/s10064-025-04513-7.

[79] Agliardi, F., Crosta, G. B., & Frattini, P. (2009). Integrating rockfall risk assessment and countermeasure design by 3D modelling techniques. Natural Hazards and Earth System Science, 9(4), 1059–1073. doi:10.5194/nhess-9-1059-2009.

[80] Yepes, J., García-González, C., & Franesqui, M. A. (2020). Rockfall hazard mitigation on infrastructures in volcanic slopes using computer-modelled ditches. Transportation Geotechnics, 25, 100402. doi:10.1016/j.trgeo.2020.100402.